



ELSEVIER

Available online at www.sciencedirect.com

European Journal of Cell Biology ■■■■■ ■■■■■

European Journal
of Cell Biologywww.elsevier.de/ejcb

Dictyostelium discoideum chemotaxis: Threshold for directed motion

Loling Song^{a,b}, Sharvari M. Nadkarni^a, Hendrik U. Bödeker^{a,c}, Carsten Beta^{a,d},
Albert Bae^{a,d}, Carl Franck^a, Wouter-Jan Rappel^e, William F. Loomis^f,
Eberhard Bodenschatz^{a,d,*}

^aLaboratory of Atomic and Solid State Physics, Department of Physics, Cornell University, Ithaca, NY 14853, USA

^bDepartment of Cell Biology, Harvard Medical School, Boston, MA, USA

^cInstitut für Angewandte Physik, Westfälische Wilhelms-Universität Münster, Germany

^dMax Planck Institute for Dynamics and Self-Organization, Am Fassberg 11/Turm 2, D-37077 Göttingen, Germany

^eDepartment of Physics and Center for Theoretical Biological Physics, University of California, San Diego, La Jolla, CA 92093, USA

^fDivision of Biological Sciences, University of California, San Diego, La Jolla, CA 92093, USA

Abstract

The chemotactic response of *Dictyostelium discoideum* cells to stationary, linear gradients of cyclic adenosine 3',5'-monophosphate (cAMP) was studied using microfluidic devices. In shallow gradients of less than 10^{-3} nM/ μ m, the cells showed no directional response and exhibited a constant basal motility. In steeper gradients, cells moved up the gradient on average. The chemotactic speed and the motility increased with increasing steepness up to a plateau at around 10^{-1} nM/ μ m. In very steep gradients, above 10 nM/ μ m, the cells lost directionality and the motility returned to the sub-threshold level. In the regime of optimal response the difference in receptor occupancy at the front and back of the cell is estimated to be only about 100 molecules.

© 2006 Published by Elsevier GmbH.

Keywords: Chemotaxis; *Dictyostelium discoideum*; Microfluidics

Introduction

How a cell senses, responds, and moves towards a chemical signal is central to many biological and medical phenomena including morphogenesis, immune response, and cancer metastasis. Over the past thirty years, major research efforts were undertaken to advance the understanding of the complex phenomenon of chemotaxis – the directional movement of a cell

toward a chemical source (Parent and Devreotes, 1999; Postma et al., 2004; van Haastert and Devreotes, 2004). Chemotaxis has been investigated for a variety of biological systems ranging from prokaryotic cells to mammalian leukocytes and neutrophils. Among the most prominent model organisms for the study of chemotactic behavior is the eukaryotic microorganism *Dictyostelium discoideum* (Arkowitz, 1999; Chisholm and Firtel, 2004; Firtel and Meili, 2000; Kimmel and Parent, 2003; Meima and Schaap, 1999; Williams and Harwood, 2003). The last decade has witnessed a rapid advance in deciphering the molecular pathways that govern the directional response of a cell to chemoattracting agents (Parent and Devreotes, 1999; van

*Corresponding author. Max Planck Institute for Dynamics and Self-Organization, Am Fassberg 11/Turm 2, D-37077 Göttingen, Germany. Tel.: +49 551 5176 300; fax: +49 551 5176 302.

E-mail address: eberhard.bodenschatz@ds.mpg.de (E. Bodenschatz).

Haastert and Devreotes, 2004). However, the overall picture that links the molecular details of intracellular signaling to the macroscopic movement of cells is only beginning to emerge. Systematic observations of chemotactic behavior in precisely controlled and tunable environments are needed to complement the progress in unraveling the biochemical pathways.

In the typical chemotaxis assays, concentration profiles are established by diffusion from a chemical source through porous media or a small gap to a sink (Boyden, 1962; Cutler and Munoz, 1974; Fisher et al., 1989; Nelson et al., 1975; Zicha et al., 1991; Zigmond, 1974, 1977). In most cases, the concentration profile is established slowly and continues to change over time. One notable exception is the design by Fisher et al. (1989) where temporally stable gradients were established by running solutions of different concentrations through semipermeable fibers embedded in an agarose gel. All of these chambers have the disadvantage that they do not allow the removal of any chemicals released by the cells themselves. This can significantly influence the chemical environment of the cells. Microfluidic devices combine a number of features that make them optimally suited for the study of chemotactic behavior. Aside from allowing a precise manipulation of the concentration profile (Chiu et al., 2000; Jeon et al., 2000, 2002) and reducing the transition time to establish a stable linear gradient to the order of a few seconds or less, microfluidic devices can also control the concentration of substances released by the cells themselves and thus replace a dynamically changing concentration distribution with an externally controllable chemical environment.

So far, microfluidic devices have been applied to the migration of neutrophils (Lin et al., 2004), bacteria (Thar and Kuhl, 2003), and cancer cells (Wang et al., 2004). Here, we use microfluidic techniques to study *Dictyostelium* chemotaxis in spatially linear and temporally stable cAMP gradients. In the device, stable gradients can be maintained as long as required. The concentration profile was verified by three-dimensional 2-photon imaging techniques and numerical finite-element simulations.

The experiments showed a threshold for the chemotactic response at a gradient value of $dc/dy \equiv \nabla c \approx 10^{-3} \text{ nM}/\mu\text{m}$. Above threshold, the motion was determined by the absolute steepness of the gradient of the chemoattractant, i.e., independent of the local concentration. The chemotactic speed and the motility increased with increasing steepness of the gradient until $\nabla c \approx 10^{-1} \text{ nM}/\mu\text{m}$; no further increase of the chemotactic response was observed in steeper gradients up to $\nabla c \approx 1 \text{ nM}/\mu\text{m}$. In gradients above $\nabla c \approx 10 \text{ nM}/\mu\text{m}$, the cells lost directionality and the motility returned to the sub-threshold level. An estimate of cAMP receptor occupancy as a function of gradient

steepness offers a possible explanation. It shows that in the regime of optimal response, the difference between front and back receptor occupancy is only about 100 molecules, whereas for very steep gradients saturation of the cell surface receptors suppresses a chemotactic response.

Materials and methods

Experimental setup

We used a modified version of the microfluidic pyramidal network pioneered by Jeon et al. (2000) to join a solution of cAMP with developmental buffer in a cascade mixing procedure as described by Rhoads et al. (2005). A schematic diagram of the pyramidal device is shown to scale in Fig. 1. Solutions of minimal (zero) and maximal (c_{max}) cAMP concentrations were introduced into the device through two inlets. At each bifurcation in the network, the flow was parted into an upper and a lower branch and diffusively mixed with the flow from the neighboring channels. Consequently, well defined concentration steps were built up with high precision before all branches were finally merged in a single channel to produce a linear gradient perpendicular to the direction of the flow. The length, width, and height of the channel were $l = 5 \text{ mm}$, $w = 525 \mu\text{m}$, and $h = 50 \mu\text{m}$, respectively. An automated syringe pumping system (Harvard apparatus PHD 2000 infusion pump with 500 μl Hamilton gastight syringes) was used to maintain a steady flow through the device. During the recording of experimental data, the flow speed in the main channel was $650 \mu\text{m}/\text{s}$, which was high enough to ensure a stable concentration gradient over the entire length of the channel but low enough so that the cells in

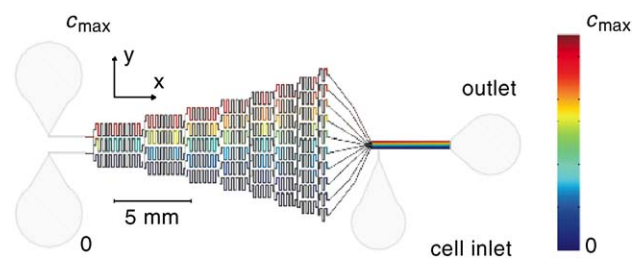


Fig. 1. Layout of the microfluidic channel network used to generate a linear concentration gradient. The color coding displays the concentration from a two-dimensional numerical simulation of the Navier–Stokes and drift-diffusion equation in the shown geometry using FEMlab 3.1. Black lines mark in- and outlets that were not part of the numerical simulation. Parameters: density $\rho = 10^{-12} \text{ g}/\mu\text{m}^3$, kinematic viscosity $\nu = 10^6 \mu\text{m}^2/\text{s}$, inflow velocity $v = 3250 \mu\text{m}/\text{s}$, inflow concentrations: zero and $c_{\text{max}} = 2 \text{ nM}$, cAMP diffusivity $D = 400 \mu\text{m}^2/\text{s}$ (Bowen and Martin, 1964), no-slip and isolating boundary conditions except for inlet and outlet.

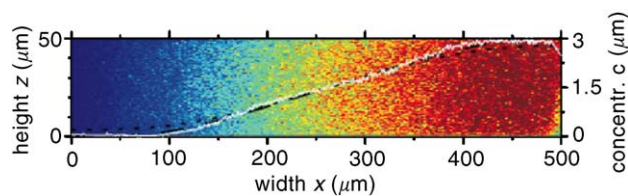


Fig. 2. Concentration profile cross section of the gradient channel as a function of height. Colored surface plot (with scale on the left side): distribution of cAMP concentration at the entrance of the main channel of the microfluidic device measured by 2-photon microscopy using fluorescein. White solid line (with scale on the right side): resulting concentration profile averaged in z -direction. Black lines: concentration profile at the beginning (dashed line) and the end (dotted line) of the channel as a result of three-dimensional simulations.

the channel were not washed away. This constant flow also provided sufficient oxygen and disposal of all substances released by the cells. For the majority of the investigations conducted in this report, the gradient was established between no cAMP on one side of the channel and a maximal level c_{\max} of cAMP on the other side of the channel. The stability of the concentration gradient over the length and depth of the channel was directly tested using 2-photon microscopy. The concentration at every position in the device was constant in the vertical dimension (Fig. 2). Furthermore, we have verified that the concentration profiles are temporally stable by measuring the gradient before and after the start of the experiments (data not shown). The results showed excellent agreement with numerical simulations of the incompressible Navier–Stokes equation coupled to the convection–diffusion equation for the concentration field. As seen in Fig. 2, due to the limited lateral size of the gradient device, a concentration plateau was observed close to the channel boundaries. In the center, a linear gradient was measured over a length of 300 μm across the channel. Therefore, the analysis of cell motion was limited to this interval.

Cell culture

We used the AX3-derived strain WF38, which expresses a green fluorescent protein fused to the pleckstrin-homology (PH) domain of the cytosolic regulator of adenylyl cyclase (CRAC) which was kindly provided by P. N. Devreotes, Johns Hopkins University. The cells were grown in shaking suspension of HL5 nutrient solution (56 mM glucose, 10 g/l peptic peptone, 5 g/l yeast extract, 2.5 mM Na_2HPO_4 , 2.6 mM KH_2PO_4 , penicillin, streptomycin, gentamycin, pH 6.5) and renewed from frozen stock every four weeks. For all experiments, 2 ml of cell suspension at 2×10^6 cells/ml were concentrated by centrifugation at 100g for 20 s. The supernatant was removed. The cells were then resuspended, loaded into the main channel, and allowed to

settle and attach to the bottom glass coverslip for half an hour. Care was taken to avoid the formation of cell clusters and uneven distributions throughout the loading process. After a 4-h starvation period in slowly running buffer solution (5 mM Na_2HPO_4 , 5 mM KH_2PO_4 , 2 mM MgSO_4 , and 0.2 mM CaCl_2 , pH 6.2, flow speed of about 320 $\mu\text{m/s}$) in which the cells were able to signal each other, a cAMP concentration profile was established in the main channel within 30 s. A series of experiments was performed with gradients between zero and different maximal levels of cAMP, $c_{\max} = 10^{-3}$ to 10^4 nM, in steps of one order of magnitude. With the gradient extending over 300 μm this gave $\nabla c = 3.3 \times 10^{-6}$ to 33 nM/ μm . Additionally, two measurements with a spatially homogeneous concentration were performed, where the cAMP concentration was fixed at $c = 0$ and 100 nM, respectively. For each experiment a new gradient device was produced and the gradient was verified by measurement of the fluorescence from a small amount of fluorescein in the solution. Due to the high precision of the microfabrication process, different devices had equal performance.

Image acquisition and data analysis

For each experiment, cellular dynamics were recorded for the first hour following the establishment of the gradient in a region close to the inlet of the main channel (Fig. 3) using an inverted wide field Olympus IX–71 microscope coupled to a Qimaging Retiga EXI firewire CCD camera. We used a 10 \times dry objective to capture the whole width of the channel in a 1360 \times 1360 pixel frame. Unless otherwise noted, images were taken at 30-s intervals. The trajectories of cells were extracted from the experimental data using the following procedure: the phase-contrast information was transformed into intensity information by applying a Sobel edge detection, followed by a blurring of the individual images. The centers of the cells were then identified as the centers of connected regions with intensity above a given threshold. From the positions in the individual frames, two-dimensional trajectories were determined using a nearest-neighbor particle tracking algorithm. The quality of this procedure was checked by comparing with manually obtained tracks.

The cell coordinates (x, y) were measured in the region of constant gradient, i.e., in a 300 μm wide interval located about 100 μm from each side. The cell motion was characterized in terms of cell velocity components parallel ($v_x(t) = dx(t)/dt$) and perpendicular ($v_y(t) = dy(t)/dt$) to the direction of the flow. In the presence of a gradient, $v_y^{(t)}$ points in the direction of increasing concentration. The chemokinetic response was quantified by the motility $M(t) = \sqrt{v_x^2 + v_y^2}$ (for definition of the coordinates see also Fig. 3). In the case

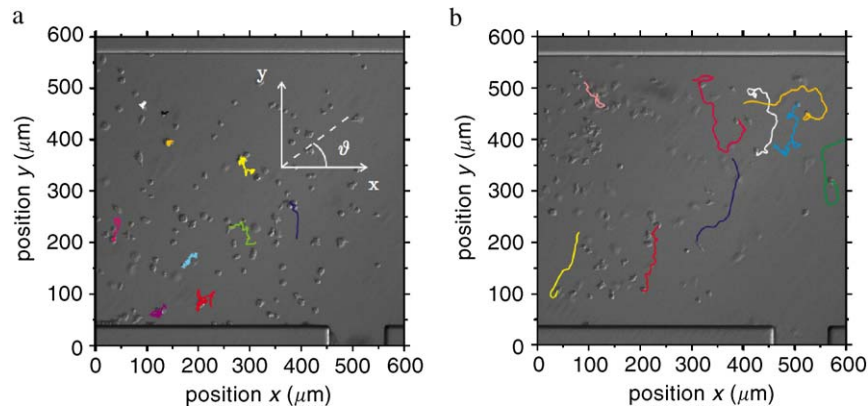


Fig. 3. Initial state and trajectories of cells (a) for a developmental buffer solution and (b) for a cAMP gradient from 0 to $c_{\max} = 10$ nM ($\nabla c = 0.033$ nM/ μm).

of a gradient, v_y is the chemotactic velocity. All quantities were approximated using a first order finite-difference scheme. Unless otherwise stated, positions were evaluated at a time interval of $\Delta t = 30$ s. The results were insensitive to a variation of Δt from 20 s to 1.5 min. To further characterize the motion, the propagation angle ϑ with respect to the direction of the flow was measured (see Fig. 3). At least 50 cells were analyzed in each experiment.

The above quantities constitute the most elementary way to characterize cell motion. Contrary to other quantities like the chemotactic index, chemotactic efficiency etc., they involve no nonlinear transformations.

Results

Cell motion in absence of a cAMP gradient

The velocity components and the motility of a large number of cells were determined and statistically analyzed for two spatially uniform concentration profiles across the channel. Due to the spatial isotropy in these cases, the statistics of the velocities should not depend on the position of the cells in the channel.

In the absence of cAMP, the cells were not at rest, but performed a random type of motion (see tracks in Fig. 3a). The average motility was $M = 4.19$ $\mu\text{m}/\text{min}$, while the velocity components took average values close to zero (Table 1). The distributions of the velocity components v_x and v_y were found to be symmetric, and the propagation angles were uniformly distributed, as shown in Figs. 4a and 5a, respectively. No preferred direction was observed. This confirms that cell motion is not influenced by flow-induced shear forces in our setup. In a similar manner, we examined cells at 100 nM homogeneous cAMP concentration. A slightly higher average motility of $M = 5.47$ $\mu\text{m}/\text{min}$ was found and,

Table 1. Motility and velocity components in absence of cAMP and for a constant cAMP concentration of 100 nM

c (nM)	M ($\mu\text{m}/\text{min}$)	v_x ($\mu\text{m}/\text{min}$)	v_y ($\mu\text{m}/\text{min}$)
0	4.19 (± 2.68)	0.14 (2.65)	0.04 (± 2.81)
100	5.47 (± 2.94)	-0.40 (± 3.57)	-0.18 (± 3.95)

The values in parentheses are the standard deviations of the average velocities of individual cells.

again, the average velocity components were small (Table 1). The velocities of individual cells showed large variations. This is quantified by the standard deviations of the average velocities of individual cells (Table 1). Finally, we analyzed the motility of individual cells for periodicity in time. No dominant time scale for the fluctuations could be found (data not shown).

Cell migration in linear gradients of cAMP

A directional response was found once the gradient steepness exceeded a threshold value of $\nabla c \approx 10^{-3}$ nM/ μm . Typical cell tracks for this case are depicted in Fig. 3b for $\nabla c = 0.033$ nM/ μm . The distribution of velocity components and propagation angles are shown in Figs. 4b and 5b. While the v_x distribution is similar to the non-gradient case, the v_y distribution is strongly skewed into the direction of the gradient. The angular distribution exhibits a pronounced peak at $\vartheta = 90^\circ$, corresponding to the direction of the gradient.

The results for the average v_x and v_y velocities as well as the average motility as a function of concentration gradients are summarized in Fig. 6. These values were obtained by dividing the region of linear gradient into five equal bins and by evaluating the cell motion separately within the three middle bins (the two outer bins were eliminated to minimize edge effects). The velocities in these bins were found to be constant within 50% and showed no systematic bias at lower or higher background concentrations (data not shown). The bars

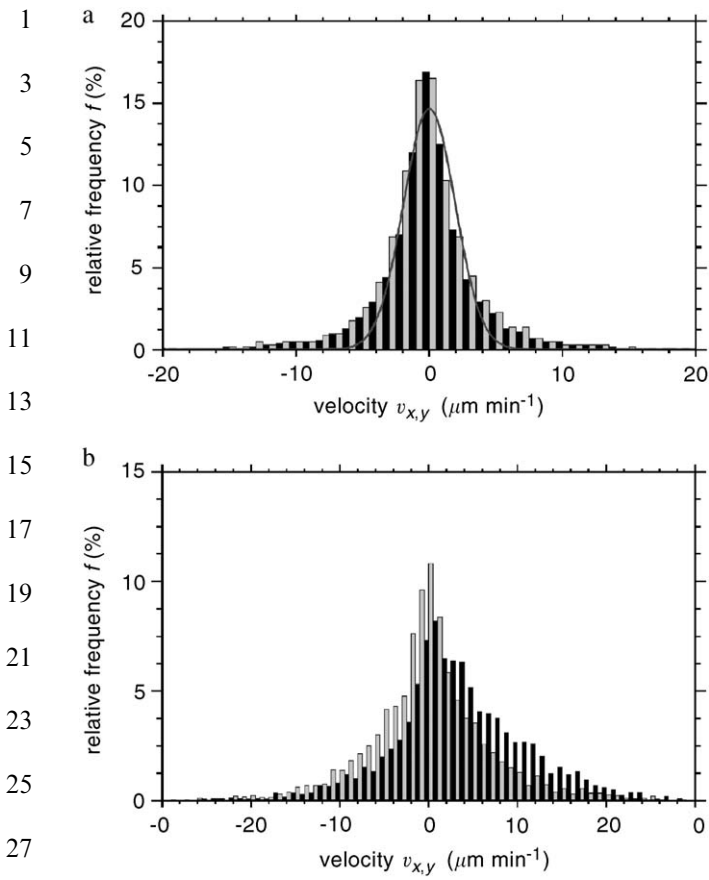


Fig. 4. Histograms of the distribution of the velocity components v_x (gray) and v_y (black) (a) for a developmental buffer solution and (b) for a cAMP gradient from 0 to $c_{\text{max}} = 10 \text{ nM}$ ($\nabla c = 0.033 \text{ nM}/\mu\text{m}$). Each bin is originally twice as wide as shown in the plot, the black bins have been shifted to the right half a bin-width for better visualization. A Gaussian distribution was fitted to the v_y distribution in (a), showing a pronounced deviation in the regions of the tails.

indicate the range of mean velocity values obtained by this binning procedure. For cAMP gradients from $\nabla c = 10^{-6}$ to $10^{-3} \text{ nM}/\mu\text{m}$, no significant directed response was observed. The average motility showed no dependence on the local cAMP concentration and was similar to the case without cAMP. Above a threshold of $\nabla c \approx 10^{-3} \text{ nM}/\mu\text{m}$, both motility and chemotactic velocity increased significantly with increasing gradient. For concentration gradients $\nabla c \approx 0.33\text{--}3 \text{ nM}/\mu\text{m}$, motility and chemotactic velocity were approximately independent of the gradient. Note that the average motility for these gradients ($\approx 9 \mu\text{m}/\text{min}$) is comparable to the motility observed in cells that had been developed to peak motility by external pulsing of cAMP (Stepanovic et al., 2005; Wessels et al., 2000, 2004). Thus, cells developed in our microfluidic device are at a similar developmental stage as cells developed using traditional pulsing techniques. For even higher gradients, i.e., $\nabla c > 3.3 \text{ nM}/\mu\text{m}$, both quantities decayed

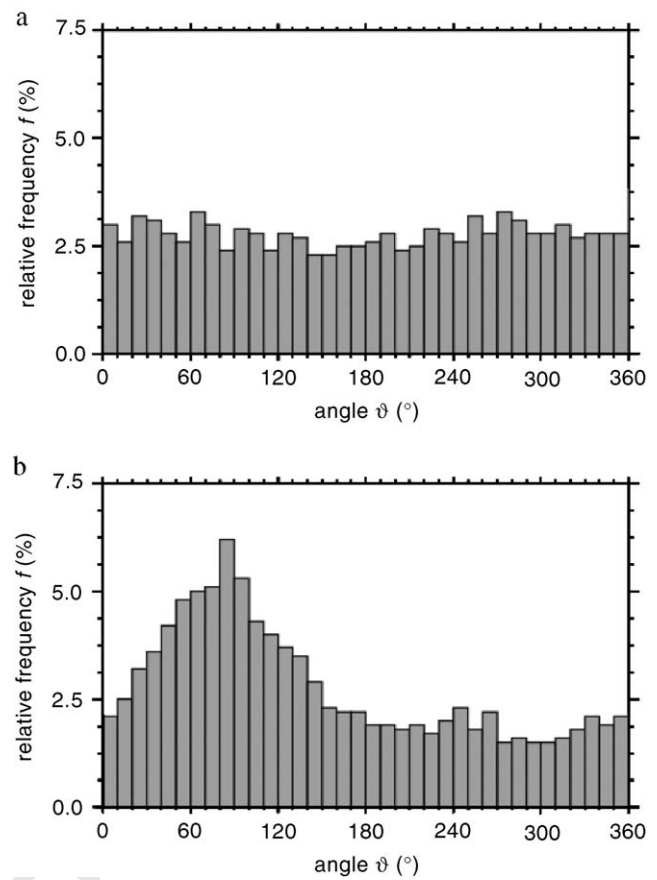


Fig. 5. Histograms of the distribution of propagation angles (a) for a developmental buffer solution and (b) for a cAMP gradient from 0 to $c_{\text{max}} = 10 \text{ nM}$ ($\nabla c = 0.033 \text{ nM}/\mu\text{m}$).

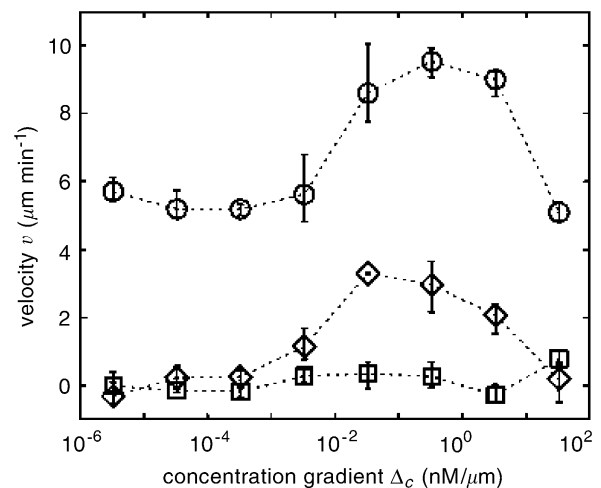


Fig. 6. Average velocity components v_x (squares) and v_y (chemotactic velocity, diamonds) as well as motility (circles) measured for different cAMP gradients. The bars indicate the spread in velocities (see text).

rapidly to sub-threshold values. As in the case of constant cAMP concentration, no evidence for pulsatile motion could be found (data not shown).

Discussion

cAMP and chemotactic motion

The chemotactic response was studied both as a function of cAMP concentration and gradient steepness. We found directed motion above a lower threshold of $\nabla c \approx 10^{-3}$ nM/ μm and below an upper threshold of $\nabla c \approx 10$ nM/ μm (Fig. 6). We propose an explanation for the upper and lower thresholds by considering the occupancy of cAMP receptors on the cell membrane. As shown in the Supplementary Material (online version only), the adsorption and desorption processes are reaction limited. Therefore, chemical equilibrium can be assumed and the relative receptor occupancy is given by $\theta = c(c + K_d)^{-1}$ with c the cAMP concentration and K_d the equilibrium dissociation constant. Using this relationship, the receptor occupancy at the front and back of the cell can be estimated. We consider a cell of 10 μm in length with 25,000 receptors at the front and back, respectively, located in the middle of the device (Dormann et al., 2001). The relative occupancies and the difference in number of occupied receptors at the front and back are summarized in Table 2 for different gradients. For concentration values well below K_d , the difference in occupied receptors at the front and back remains roughly constant for different locations in the same gradient, even though the absolute number of occupied receptors changes significantly. For higher concentrations, however, this difference decreases as the cells move up the gradient.

Below the threshold of $\nabla c \approx 10^{-3}$ nM/ μm , the difference in occupancy is of the order of one receptor and less than 0.1% of all receptors are occupied. It can be concluded that too few cAMP molecules hit the receptors to allow the cells to distinguish different concentration levels at its front and back. For the lowest gradient value where directed motion is observed ($\nabla c = 3.3 \times 10^{-3}$ nM/ μm), we find the number of occupied receptors to be 128 and 120 at the front and

back, respectively. For larger gradients, the difference in the number of occupied receptors increases to reach a maximum for $\nabla c = 0.33$ nM/ μm . Above $\nabla c \approx 10$ nM/ μm , this difference drops dramatically and about 98% of all receptors are occupied. This corresponds to the regime, where a complete loss of directional response was observed. A steep gradient corresponds to high local cAMP concentrations over large parts of the channel. Therefore, the loss of directionality can be explained by saturation of the receptors. Others have proposed that at high cAMP concentrations, an overall desensitization of cAMP receptors may occur through alteration in binding properties or covalent modification (Janssens and van Haastert, 1987).

Note that the interplay of geometry and flow speed can lead to modifications of the concentration profile in the immediate vicinity of a cell. For the flow parameters of the experiments presented here, this effect has been minimized and the concentration variation due to flow effects was less than 20% (data not shown).

Influence of cAMP on motility

In the absence of cAMP as well as in a spatially constant cAMP concentration, *Dictyostelium* cells move with a constant basal motility and perform a random-type motion. Similar dynamics were observed for shallow gradients below threshold as well as for very steep gradients (below $\nabla c \approx 10^{-3}$ nM/ μm and above $\nabla c \approx 10$ nM/ μm). Since secreted cAMP is washed away by the continuous fluid flow, we assume that an intrinsic mechanism is responsible for the random motion that does not depend on intercellular signaling. Above threshold, an increase in motility is observed (Fig. 6). It can be assumed that this increase reflects the increasing chemotactic velocity, which is superimposed on the basal motility. However, a weak dependence of the random basal motion on local cAMP concentration cannot be excluded from the present data.

Comparison with previous work

We observe a directional response for gradients steeper than $\nabla c \approx 10^{-3}$ nM/ μm . This is in excellent agreement with the value of 3.6×10^{-3} nM/ μm reported by Mato et al. (1975). The maximum chemotactic response between $\nabla c \approx 0.01$ and 0.1 nM/ μm matches the observation by Varnum and Soll (1984) who found a maximal chemotactic velocity at $\nabla c \approx 0.01$ nM/ μm . A similar value of $\nabla c \approx 0.05$ nM/ μm was also reported by Vicker et al. (1984). The rapid decrease in chemotactic velocity for steep gradients, i.e. high cAMP concentrations, was also reported by Varnum and Soll (1984). For shallow gradients, however, our results do not agree with the data of Varnum and Soll, who observed a

Table 2. Occupancy rates at the front (θ_f) and back (θ_b) and difference in the numbers of occupied receptors between front and back of a cell in the middle of the gradient (at midpoint concentration) with $N = 25,000$ sites in each half and $K_d = 100$ nM (Dormann et al., 2001)

∇c (nM/ μm)	c_m (nM)	θ_b (%)	θ_f (%)	$(\theta_f - \theta_b) \times N$
3.3×10^{-5}	0.005	0.005	0.005	0
3.3×10^{-4}	0.05	0.048	0.052	1
3.3×10^{-3}	0.5	0.48	0.51	8
0.033	5	4.6	4.9	75
0.33	50	32.6	34.1	375
3.3	500	82.9	83.8	225
33	5000	98.0	98.1	25

constant level of high motility also for small cAMP concentrations. This can be explained by the differences in experimental setup. Most of the previous work was carried out in gradient chambers where concentration profiles build up through pure diffusion. Waste products and chemical signals secreted by the cells can accumulate inside these chambers. In a microfluidic device, the effect of waste products and mutual signaling between cells is significantly decreased due to a continuous fluid flow. This leads to different results in the regime of low cAMP concentrations.

Fisher et al. (1989) have minimized the effect of secreted substances by using appropriate mutants. For comparison, we have translated our data into accuracy of chemotaxis (Fisher et al., 1989; Mardia and Jupp, 2000) (data not shown). The maximal chemotactic response occurs for similar gradient values (Fig. 5 in Fisher et al., 1989). However, Fisher et al. (1989) reported a continuous increase in chemotactic motion with increasing gradient, while we observed a pronounced lower threshold at $\nabla c \approx 10^{-3}$ nM/ μm .

Conclusions

Microfluidic techniques were introduced to study chemotactic motion of *Dictyostelium* cells in gradients of cAMP. A number of basic questions of chemotactic behavior were revisited, using the particularly well-suited features of microfluidic devices.

Our experimental results suggest that the chemotactic movement of cells in gradients of cAMP is determined by both stochastic and deterministic components. Deterministic motion is induced by the presence of a cAMP gradient. The effective speed of motion depends on the absolute and not on the relative value of the gradient. The stochastic component is always present and seems to be independent or, at most, weakly influenced by the presence of cAMP. Although the experimental data give no clear proof of two distinct mechanisms for the two aspects of cell behavior, a separation of the dynamics into deterministic and stochastic components seems meaningful.

A persistent stochastic contribution to the movement of a cell could reduce its efficiency in reaching a desired destination. However, cells are able to aggregate as long as the averaged velocity over time is directed into the correct half-plane (Dallon and Othmer, 1997). Furthermore, situations in a real biological environment can be imagined where the path of a cell is obstructed and a stochastic contribution to the movement may actually help the cell finding its way around larger obstacles or through complex geometries.

For gradients close to the lower threshold ($\nabla c \approx 10^{-3}$ nM/ μm) the difference in receptor occupancy

was estimated to be only in the order of ten molecules. This raises two important questions: first, how long does it take a cell to measure the occupancy of its receptors in order to eliminate the influence of noise and large offsets, and second, how can a small difference in receptor occupancy lead to a strongly amplified downstream response? The small numbers suggest that stochastic effects on the shot-noise level play a role in chemotactic gradient sensing. However, most current models are based on continuum approximations (Meinhart and Gierer, 2000; Postma and van Haastert, 2001) and the development of a stochastic approach is only beginning to emerge (Ishii et al., 2004).

Dedication

We dedicate this study to Günther Gerisch on the occasion of his 75th birthday. The pioneering studies in his laboratory on chemotaxis in *Dictyostelium* were the inspiration for our efforts. His emphasis on accurate, quantitative measurements generated a firm foundation for further advancements.

Acknowledgments

A. Bae, E. Bodenschatz, L. Song, S. Nadkarni, W.J. Rappel and W.F. Loomis are grateful for the support by the National Science Foundation through the Biocomplexity program (NSF MCB 0083704) and through Cornell's Nanobiotechnology Center (NSF ECS 9876771), A. Bae, C. Beta and E. Bodenschatz for the support by the Max Planck Society, A. Bae and C. Franck for facilities use in the Cornell Center for Material Research (NSF MRSEC DMR 0079992), W.J. Rappel for the support from the NSF PFC-sponsored Center for Theoretical Biological Physics (Grants No. PHY-0216576 and PHY-0225630), and H.U. Bödeker is grateful for financial support through postgraduate fellowships by DFG and DAAD. We thank Herbert Levine for many fruitful discussions as well as Danny Fuller for his expertise and help in *Dictyostelium* cell cultures and strains. We thank Dan Rhoads for the design of the first microfluidic devices and Charles Hagedon, Ismael Rafols, and Danica Wyatt for their helpful contributions at various stages of this project. Thanks also go to Abraham Stroock for discussions on microfluidics, to Katharina Schneider and Duane Loh for assisting in the experiments, and to Günther Gerisch for many helpful suggestions in the preparation of this manuscript.

1 Appendix A. Supplementary material

3 The online version of this article contains additional
5 supplementary data. Please visit [doi:10.1016/
7 j.ejcb.2006.01.012](https://doi.org/10.1016/j.ejcb.2006.01.012)

11 References

- 13 Arkowitz, R.A., 1999. Responding to attraction: chemotaxis
15 and chemotropism in *Dictyostelium* and yeast. *Trends Cell
17 Biol.* 9, 20–27.
- 19 Bowen, W.J., Martin, H.L., 1964. The diffusion of adenosine
21 triphosphate through aqueous solutions. *Arch. Biochem.
23 Biophys.* 107, 30–36.
- 25 Boyden, S., 1962. The chemotactic effect of mixtures of
27 antibody and antigen on polymorphonuclear leukocytes. *J.
29 Exp. Med.* 115, 453–459.
- 31 Chisholm, R.L., Firtel, R.A., 2004. Insights into morphogen-
33 esis from a simple developmental system. *Nat. Rev. Mol.
35 Cell Biol.* 5, 531–541.
- 37 Chiu, D.T., Jeon, N.L., Huang, S., Kane, R.S., Wargo, C.J.,
39 Choi, I.S., Ingber, D.E., Whitesides, G.M., 2000. Patterned
41 deposition of cells and proteins onto surfaces by using
43 three-dimensional microfluidic systems. *Proc. Natl. Acad.
45 Sci. USA* 97, 2408–2413.
- 47 Cutler, J.E., Munoz, J.J., 1974. A simple in vitro method for
49 studies on chemotaxis. *Proc. Soc. Exp. Biol. Med.* 147,
51 471–474.
- 53 Dallon, J.C., Othmer, H.G., 1997. A discrete cell model with
55 adaptive signalling for aggregation of *Dictyostelium dis-*
57 *coideum*. *Phil. Trans. R. Soc. Lond. B* 352, 391–417.
- 59 Dormann, D., Kim, J.Y., Devreotes, P.N., Weijer, C.J., 2001.
61 cAMP receptor affinity controls wave dynamics, geometry
63 and morphogenesis in *Dictyostelium*. *J. Cell Sci.* 114,
65 2513–2523.
- 67 Firtel, R.A., Meili, R., 2000. *Dictyostelium*: a model for
69 regulated cell movement during morphogenesis. *Curr.
71 Opin. Genet. Dev.* 10, 421–427.
- 73 Fisher, P.R., Merkl, R., Gerisch, G., 1989. Quantitative
75 analysis of cell motility and chemotaxis in *Dictyostelium*
77 *discoideum* by using an image processing system and a novel
79 chemotaxis chamber providing stationary chemical gradi-
81 ents. *J. Cell Biol.* 108, 973–984.
- 83 Ishii, D., Ishikawa, K.L., Fujita, T., Nakagawa, M., 2004.
85 Stochastic modeling for gradient sensing by chemotactic
87 cells. *Sci. Technol. Adv. Mat.* 5, 715–718.
- 89 Janssens, P.M.W., van Haastert, P.J.M., 1987. Molecular basis
91 of transmembrane signal transduction in *Dictyostelium*
93 *discoideum*. *Microbiol. Rev.* 51, 396–418.
- 95 Jeon, N.L., Dertinger, S.K.W., Chiu, D.T., Choi, I.S.,
97 Stroock, A.D., Whitesides, G.M., 2000. Generation of
99 solution and surface gradients using microfluidic systems.
101 *Langmuir* 16, 8311–8316.
- 103 Jeon, N.L., Baskaran, H., Dertinger, S.K.W., Whitesides,
105 G.M., Van de Water, L., Toner, M., 2002. Neutrophil
107 chemotaxis in linear and complex gradients of interleukin-8
109 formed in a microfabricated device. *Nat. Biotechnol.* 20,
111 826–830.
- Kimmel, A.R., Parent, C.A., 2003. *Dictyostelium discoideum*
cAMP chemotaxis pathway. [http://stke.sciencemag.org/cgi/
cm/CMP_7918](http://stke.sciencemag.org/cgi/cm/CMP_7918).
- Lin, F., Saadi, W., Rhee, S.W., Wang, S.J., Mittal, S., Jeon,
N.L., 2004. Generation of dynamic temporal and spatial
concentration gradients using microfluidic devices. *Lab.
Chip* 4, 164–167.
- Mardia, K.V., Jupp, P.E., 2000. *Directional Statistics*. Wiley,
Chichester, New York.
- Mato, J.M., Losada, A., Nanjundiah, V., Konijn, T.M., 1975.
Signal input for a chemotactic response in the cellular slime
mold *Dictyostelium discoideum*. *Proc. Natl. Acad. Sci. USA*
72, 4991–4993.
- Meima, M., Schaap, P., 1999. *Dictyostelium* development –
Socializing through cAMP. *Semin. Cell Dev. Biol.* 10,
567–576.
- Meinhardt, H., Gierer, A., 2000. Pattern formation by local
self-activation and lateral inhibition. *Bioessays* 22, 753–760.
- Nelson, R.D., Quie, P.G., Simmons, R.L., 1975. Chemotaxis
under agarose: a new and simple method for measuring
chemotaxis and spontaneous migration of human poly-
morphonuclear leukocytes and monocytes. *J. Immunol.*
115, 1650–1656.
- Parent, C.A., Devreotes, P.N., 1999. A cell's sense of direction.
Science 284, 765–770.
- Postma, M., van Haastert, P.J.M., 2001. A diffusion-translo-
cation model for gradient sensing by chemotactic cells.
Biophys. J. 81, 1314–1323.
- Postma, M., Bosgraaf, L., Looovers, H.M., van Haastert,
P.J.M., 2004. Chemotaxis: signalling modules join hands at
front and tail. *EMBO Rep.* 5, 35–40.
- Rhoads, D.S., Nadkarni, S.M., Song, L., Voeltz, C., Bod-
enschatz, E., Guan, J.L., 2005. Using microfluidic channel
networks to generate gradients for studying cell migration.
Methods Mol. Biol. 294, 347–357.
- Stepanovic, V., Wessels, D., Daniels, K., Loomis, W.F., Soll,
D.R., 2005. Intracellular role of adenylyl cyclase in
regulation of lateral pseudopod formation during *Dictyos-*
telium chemotaxis. *Eukaryot. Cell* 4, 775–786.
- Thar, R., Kuhl, M., 2003. Bacteria are not too small for spatial
sensing of chemical gradients: an experimental evidence.
Proc. Natl. Acad. Sci. USA 100, 5748–5753.
- van Haastert, P.J.M., Devreotes, P.N., 2004. Chemotaxis:
signalling the way forward. *Nat. Rev. Mol. Cell Biol.* 5,
626–634.
- Varnum, B., Soll, D.R., 1984. Effects of cAMP on single cell
motility in *Dictyostelium*. *J. Cell Biol.* 99, 1151–1155.
- Vicker, M.G., Schill, W., Drescher, K., 1984. Chemoattraction
and chemotaxis in *Dictyostelium discoideum*: myxamoeba
cannot read spatial gradients of cyclic adenosine monophos-
phate. *J. Cell Biol.* 98, 2204–2214.
- Wang, S.J., Saadi, W., Lin, F., Nguyen, C.M.-C., Jeon, N.L.,
2004. Differential effects of EGF gradient profiles on
MDA-MB-231 breast cancer cell chemotaxis. *Exp. Cell
Res.* 300, 180–189.
- Wessels, D.J., Zhang, H., Reynolds, J., Daniels, K., Heid, P.,
Lu, S.J., Kuspa, A., Shaulsky, G., Loomis, W.F., Soll,
D.R., 2000. The internal phosphodiesterase RegA is

- 1 essential for the suppression of lateral pseudopods during
2 *Dictyostelium* chemotaxis. *Mol. Biol. Cell* 11, 2803–2820.
- 3 Wessels, D., Bricks, R., Kuhl, S., Stepanovic, V., Daniels,
4 K.J., Weeks, G., Lim, C.J., Spiegelman, G., Fuller, D.,
5 Iranfar, N., Loomis, W.F., Soll, D.R., 2004. RasC plays a
6 role in transduction of temporal gradient information in the
7 cyclic-AMP wave of *Dictyostelium discoideum*. *Eukaryot.*
8 *Cell* 3, 646–662.
- 9 Williams, H.P., Harwood, A.J., 2003. Cell polarity and
10 *Dictyostelium* development. *Curr. Opin. Microbiol.* 6,
11 621–627.
- 12 Zicha, D., Dunn, G.A., Brown, A.F., 1991. A new direct-
13 viewing chemotaxis chamber. *J. Cell Sci.* 99, 769–775.
- 14 Zigmond, S.H., 1974. Mechanisms of sensing chemical
15 gradients by polymorphonuclear leukocytes. *Nature* 249,
16 450–452.
- 17 Zigmond, S.H., 1977. Ability of polymorphonuclear leuko-
18 cytes to orient in gradients of chemotactic factors. *J. Cell*
19 *Biol.* 75, 606–616.
- 20
21
22
23
24
25

UNCORRECTED PROOF